The Preparation, Characterization and Tribological Properties of TA-C:H Deposited Using an Electron Cyclotron Wave Resonance Plasma Beam Source

N.A. MORRISON[1]) (a), S. MUHL (b), S.E. RODIL (a), A.C. FERRARI (a),
M. NESLÁDEK (c), W.I. MILNE (a), and J. ROBERTSON (a)

(a) Engineering Department, University of Cambridge, Cambridge CB2 1PZ, U.K.

(b) Instituto de Investigaciones en Materiales, Universidad Nacional Autonoma de Mexico, Aptd. Postal 70-360, Coyoacan, Mexico

*(c) Institute for Materials Research, Universitaire Campus,
Limburgs Universitair Centrum, Wetenschapspark, 1, B-3590 Diepenbeek, Belgium*

(Received November 26, 1998)

A compact electron cyclotron wave resonance (ECWR) source has been developed for the high rate deposition of hydrogenated tetrahedral amorphous carbon (ta-C:H). The ECWR provides growth rates of up to 900 Å/min over a 4″ diameter and an independent control of the deposition rate and ion energy. The ta-C:H was deposited using acetylene as the source gas and was characterized in terms of its sp^3 content, mass density, intrinsic stress, hydrogen content, C–H bonding, Raman spectra, optical gap, surface roughness and friction coefficient. The results obtained indicated that the film properties were maximized at an ion energy of approximately 167 eV, corresponding to an energy per daughter carbon ion of 76 eV. The relationship between the incident ion energy and film densification was also explained in terms of the subsurface implantation of carbon ions into the growing film.

1. Introduction

Diamond-like carbon (DLC) films have attracted considerable interest worldwide as a consequence of their smoothness, low coefficient of friction, high hardness, broad optical transparency and extreme chemical and biological inertness [1 to 5]. This material is characterized by a high fraction of sp^3 hybridized sites and may be found in either a hydrogenated (a-C:H) or an unhydrogenated (a-C) state.

It is widely known that the sp^3 bonded fraction within these films may be maximized during deposition using a source of medium energy ions [4]. Indeed, the most highly sp^3 bonded form of amorphous carbon, known as tetrahedrally bonded amorphous carbon (ta-C) has been prepared using a filtered beam of C^+ ions produced from a solid carbon source [6]. DLC containing up to 85% sp^3 bonded carbon has been deposited in this fashion. In contrast, the majority of the paper reported on the deposition of hydrogenated DLC has involved plasma-enhanced chemical vapour deposition using a number of different hydrocarbon precursors [3, 7]. Conventional plasma deposition processes result in films with relatively low sp^3 hybridized carbon contents. This has been attributed to the low concentration of ionized species present within the film-forming

---

[1]) Corresponding author: e-mail: nam22@eng.cam.ac.uk; Fax: +(44)1223 332662

flux due to the high deposition pressure and low plasma density [7]. Consequently, the hydrogenated analogue of ta-C, known as ta-C:H, has only been produced when the degree of ionization within the deposition flux has been substantially increased relative to that obtained in conventional plasma processing discharges [8]. This has been achieved previously, by the use of a low pressure, magnetically confined, capacitively coupled, rf plasma beam source [4, 8]. However, this technique is not suitable for coating large areas and gives a relatively low deposition rate of about 100 Å/min. More recently, an alternative method of depositing ta-C:H has been reported [9]. This has involved the use of an electron cyclotron wave resonance (ECWR) plasma beam source and has permitted uniform coating over large areas at high rates.

2. Electron Cyclotron Wave Resonance

An ECWR source comprises a single-turn inductively-coupled rf (13.56 MHz) discharge with a superimposed static transverse magnetic field. During operation, the application of a magnetic field results in the formation of an electrically anisotropic plasma which, according to the theory for the propagation of electromagnetic radiation in an electrically anisotropic medium, splits a linearly polarized wave with wave vector $\mathbf{k}$, parallel to the superimposed magnetic field $\mathbf{B}$, into two circularly polarized waves [10 to 12]. The dispersion relations for the right and left-hand polarized waves are given by

$$n_r^2 = 1 - \frac{\left(\frac{\omega_p^2}{\omega^2}\right)}{\left[1 - \left(\frac{\omega_c}{\omega}\right)\right]} \, , \tag{1}$$

and

$$n_l^2 = 1 - \frac{\left(\frac{\omega_p^2}{\omega^2}\right)}{\left[1 + \left(\frac{\omega_c}{\omega}\right)\right]} \, , \tag{2}$$

where n_r and n_l are the refractive indices of the right and left-hand polarized waves, respectively, and ω_p, ω and ω_c are the plasma, generator and electron cyclotron frequencies, respectively.

Whilst the left-hand polarized wave is subject to the skin effect for all frequencies at low magnetic field strengths, the right-hand polarized wave can propagate in a frequency range below the electron cyclotron frequency [10, 11] defined by

$$\omega_c = \left(\frac{e}{m}\right) B_0 \tag{3}$$

and up to the plasma frequency described by

$$\omega_p = \left(\frac{n_e e^2}{\varepsilon_0 m}\right)^{1/2} , \tag{4}$$

where e is the charge of the electron, m is the mass of the electron, B_0 is the applied magnetic field strength, n_e is the plasma density and ε_0 is the permittivity of a vacuum. This frequency window can therefore be used to couple the rf power into the plasma.

Furthermore, as a consequence of the dispersion relation shown in equation (1), the refractive index and hence the wavelength of the right hand polarized wave may be modulated through the variation of either the plasma density, the generator frequency or the applied magnetic field strength. Eventually a condition can be reached whereby a standing wave of a half-integral multiple of the wavelength of the right-hand polarized wave fits inside the cross-section of the source normal to the symmetrical axis of the single-turn electrode. This phenomenon is known as electron cyclotron wave resonance. In this condition the magnetic field strength B_{res} can be defined as

$$B_{\text{res}} = \frac{1 + \left(\dfrac{e^2}{c^2\pi^2\varepsilon_0 m}\right)\left(\dfrac{d^2 n_{\text{e}}}{(2\kappa+1)^2}\right)}{\left(\dfrac{e}{m\omega}\right)} \, , \tag{5}$$

where e, m, ε_0, ω and n_{e} have the same meanings as described previously, c is the speed of light, d is the diameter of the single-turn electrode and the integer κ is the order of the resonance (0, 1, 2, 3... etc.) [10]. At resonance there is a strong absorption of energy by the electrons in the plasma as the rotation of the electric field vector of the right-hand polarized wave coincides with the gyration direction of the plasma electrons [12]. Hence, the plasma is heated very efficiently. Combined with a reduction in electron losses to the walls through electron cyclotron motion around the magnetic field lines, this resonant energy transfer enables high plasma densities to be achieved even for excitation frequencies of 13.56 MHz ($n_{\text{e}} \approx 10^{11}$ to 10^{13} cm^{-3} [9, 10] compared with 10^9 cm^{-3} for conventional rf based plasma processing discharges [13]). Consequently, highly ionized plasmas may be produced at both low operating powers and pressures.

3. Experimental

The ta-C:H films were deposited in a UHV reactor designed and built within these laboratories. The deposition chamber is based upon copper gasket technology and is pumped by two different pumping sets: one for chamber roughing (Leybold Heraeus D60AC rotary pump, pumping speed 75 m^3/h and a Leybold Heraeus WAU250 roots blower, pumping speed 250 m^3/h) and another for providing both the base vacuum and pumping the process gases during deposition (liquid nitrogen trapped Edwards E06 diffusion pump, pumping speed 1300 l/s). The attached ECWR plasma beam source supplied by CCR GmbH (see Fig. 1), comprises a single-turn electrode of diameter 8 cm and length 7 cm, surrounded by two copper wire Helmholtz coils which generate the static magnetic field. A grounded tungsten extraction grid may also be included.

The films were deposited over silicon and quartz substrates at room temperature as a function of both ion energy and ion current density. These two parameters were varied by either altering the magnetic field strength or the rf power, respectively, and were monitored using a Faraday cup mounted in the substrate plane. A floating double Langmuir probe was also used to measure the plasma density and electron temperature within the source. Acetylene was used as the source gas for deposition owing to its relatively simple ionization and fragmentation pattern at low pressures. Under these conditions the major products within the plasma beam source are the $C_2H_X^+$ species, because simple ionization reactions have a significantly lower appearance potential than reactions involving C≡C bond cleavage [4].
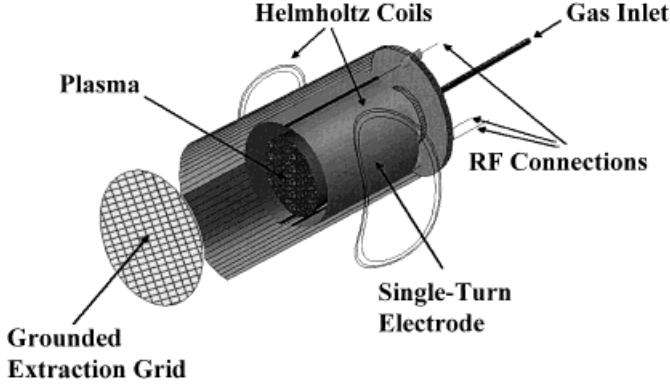
Fig. 1. Schematic of the ECWR plasma beam source

The deposited material was characterized in terms of its structural, mechanical and optical properties. The film thickness was determined by surface profilometric measurements (Sloan Dektak II) of a step formed by masking the substrate during deposition and also by ellipsometry (Gaertner Scientific L117). Ellipsometry was also used to determine the refractive index of the deposited material. The sp^2 fraction and the mass density of the films were determined by electron energy loss spectroscopy (EELS) carried out on a Vacuum Generators HB501 scanning transmission electron microscope with a dedicated parallel EELS spectrometer. The sp^2 fraction was obtained from the carbon K-edge spectrum observed between 285 and 310 eV [14]. Within this region, the ratio of the π^* peak, centered at 285 eV, and the σ^* peak found between 290 and 310 eV was determined and compared to that of graphite. The mass density was derived from the valence plasmon energy which is given by

$$E_\mathrm{p} = \hbar \left(\frac{ne^2}{\varepsilon_0 m} \right)^{1/2}, \tag{6}$$

where n is the valence electron density, ε_0 is the permittivity of a vacuum, $\hbar$ is Planck's constant and m is the effective electron mass, fitted to the plasmon energy of diamond of 34 eV.

The valence electron density was then used in order to obtain the mass density in accordance with the equation

$$n = \frac{12 \varrho N_\mathrm{A}}{m_\mathrm{C}} \left(\frac{3x_\mathrm{C} + 1}{11x_\mathrm{C} + 1} \right), \tag{7}$$

where ϱ is the mass density, N_A is Avogado's number, m_C is the mass of a carbon atom and x_C is the fraction of carbon in the film, with four electrons coming from each carbon atom and one electron from each hydrogen atom. The hydrogen content was also determined through a combination of Rutherford Backscattering and Elastic Recoil Detection Analysis measurements.

The nature of the chemical bonding within the films was determined by using an FTIR spectrometer (ATI Matteson RS1) in the 500 to 4000 cm^{-1} range. An average of 800 scans were taken per sample whilst purging the spectrometer with nitrogen. This was performed to improve the resolution of the spectra and also to inhibit the appear-

ance of bands associated with CO_2 and water vapour. Unpolarized Raman spectra were also recorded *ex situ* at room temperature in backscattering geometry. An I.S.A. Jobin-Yvon triple grating spectrometer with a liquid nitrogen cooled CCD system and an Ar ion laser (λ = 514.5 nm) was used in order to obtain spectra of resolution ≈ 3 cm^{-1}. The instrument was operated in the macro-Raman configuration in order to avoid the possibility of sample damage. The laser power during measurement was ≈ 10 mW over a 100 μm^2 area. The optical properties of the deposited material were investigated by optical absorption spectroscopy. This was achieved using an ATI Unicam UV2-200 UV-VIS spectrometer over the 185 to 910 nm wavelength range.

The stress in the deposited films was determined from the substrate radius of curvature measured both before and after deposition using a surface profilometer. These two properties are related by Stoney's equation, given by

$$\sigma = \left[\frac{Yt_s^2}{6t(1-\nu)} \right] \left[\frac{1}{R} - \frac{1}{R_0} \right], \tag{8}$$

where Y, ν and t_s are the Young's modulus, Poisson's ratio and the thickness of the substrate, respectively, t is the film thickness and R and R_0 are the substrate radii of curvature before and after deposition, respectively. The surface topography of the deposited material was investigated using a Nanoscope III Atomic Force Microscope (Digital Instruments) in tapping mode.

Tribological characterisation was performed using a ball-on-disk tribometer. Stainless steel balls (AISI 52100, 6.35 mm diameter) were used during the tests which were conducted both in air and under a controlled humidity environment. A load of 0.2 N was applied corresponding to a Hertzian contact pressure of 330 MPa. A sliding speed of 15 mm/s was used in each of the measurements.

4. Results and Discussion

Prior to the growth experiments a series of measurements were taken using the floating double probe in a nitrogen plasma. Acetylene was not used as the process gas at this stage as it is well known that the coating of the exposed probe tips leads to a perturbation of the plasma current–voltage characteristics [15]. The results, however, did indicate that the plasma density within the source was between 10^{10} and 10^{11} cm^{-3} depending upon the spatial positioning of the probe within the source, the rf power and the applied magnetic field strength. Furthermore, the measurements indicated that the electron temperature varied between 5 and 11 eV suggesting that in an acetylene plasma considerable ionization occurs through interaction with the high energy tail of the electron energy distribution.

The source rf power and the dc voltage applied to the Helmholtz coils were shown to have a profound effect upon both the mean ion energy and the ion current density. The electron cyclotron wave resonance was detected whilst monitoring the variation in ion current density with the magnetic field strength. Using acetylene as the source gas, with an rf power of 100 W and a chamber pressure of $\approx 2 \times 10^{-3}$ mbar, the fundamental resonance was observed at a coil voltage of 3.6 V which corresponded to a magnetic field strength of 13 G. However, as the rf power was increased, the plasma density also increased and a higher magnetic field strength was required in order to further maximize ion generation. In addition, the presence of the grounded extraction grid allows
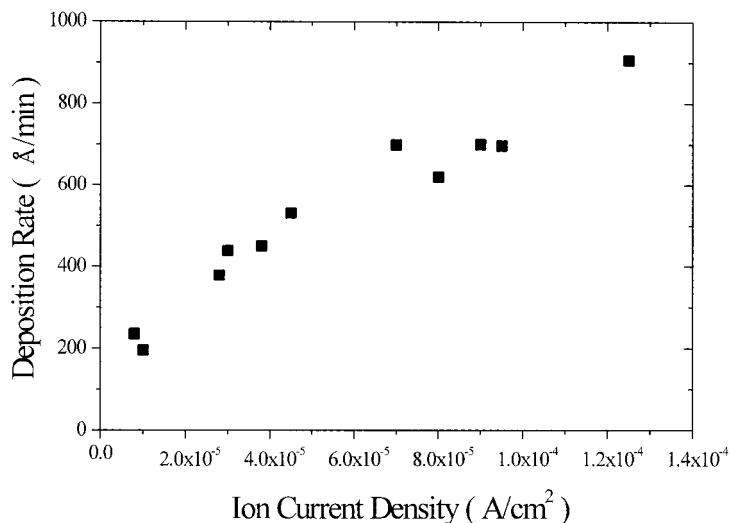
Fig. 2. Plot of the deposition rate as a function of the ion current density

some capacitive as well as inductive coupling of the plasma. Consequently, the ion energy could be controlled by varying the extent of capacitive coupling within the source as this determines the rf induced dc bias of the electrode relative to ground [4].

As shown in Fig. 2, the deposition rate was found to depend almost linearly upon the ion current density, irrespective of the variation in rf power, chamber pressure or magnetic field strength. This behavior suggests the dominance of the ion species within the growth process and may be attributed to the higher sticking coefficient for ions than radicals or neutral species. In addition, deposition rates of up to 900 Å/min were achieved at an ion current density of 1.25×10^{-4} A/cm^2, which was considerably more than the 100 Å/min obtained conventionally using the original plasma beam source [4]. Furthermore, previous results using a source of this type [9] have indicated a radial homogeneity in the deposition rate of within $\pm 5\%$ over a 4″ substrate diameter.

The properties of the deposited ta-C:H films were found to depend upon the mean ion energy of the film forming flux. Fig. 3 shows that the sp^3 fraction, film stress and optical band gap all pass through a maximum as a function of the ion energy. This maximum appears at an ion energy of ≈ 167 eV, slightly lower than the 200 eV reported in the original plasma beam source [4]. The sp^3 fraction, mass density, film stress, optical band gap and refractive index were found to be 0.77, 2.38 g/cm^3, 8 GPa, 2.1 eV and 2.45, respectively, at an ion energy of ≈ 167 eV. With the exception of the film density, these values compare reasonably well with ta-C films of similar thickness [16].

The hydrogen content was found to decrease slightly with increasing ion energy, even though the total hydrogen content within the film was found to be less than ≈ 33 at%. This was attributed to the rise in the hydrogen sputter yield with ion energy. FTIR measurements (see Fig. 4) confirmed this, as the total integrated intensity of the C–H envelope at 2750 to 3150 cm^{-1} was found to decrease with increasing ion energy. This envelope was deconvoluted into a series of Gaussian components corresponding to the different vibration modes of the C–H bond. In each case the C–H stretching modes of
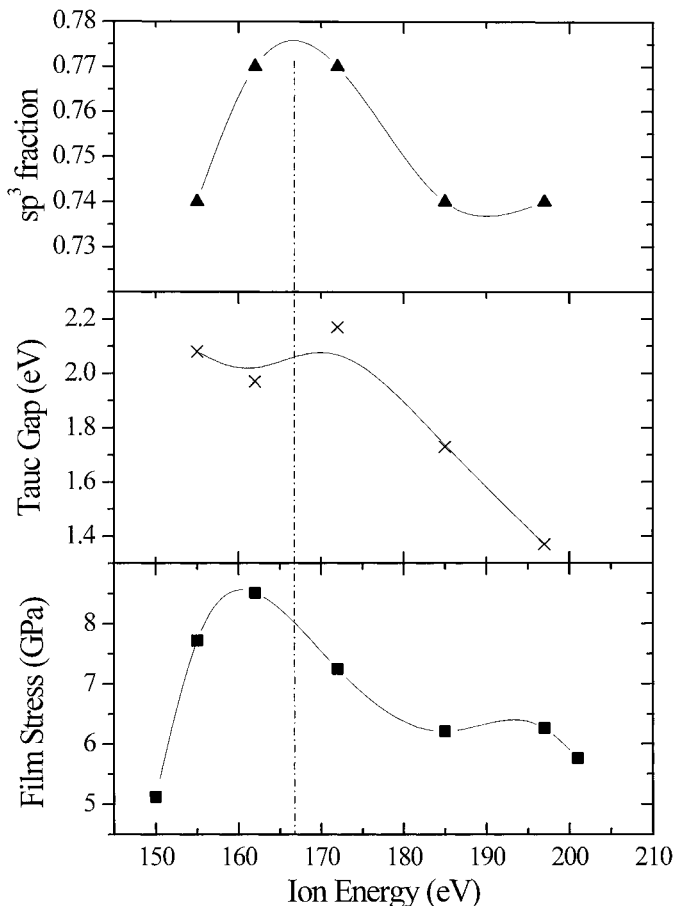
Fig. 3. Variation in film stress, Tauc gap and sp^3 fraction with ion energy

sp^3 hybridized CH and CH_2 groups were observed at 2920 and 2850 cm^{-1}, respectively. The C–H envelope, however, was significantly broadened beyond 3000 cm^{-1}. This was attributed to the presence of both olefinic and aromatic C–H bonds present within the network [17]. It is also interesting that C–C modes around 1500 cm^{-1} were observed. Here we see the clear presence of the olefinic and aromatic C=C stretches at $\approx$1580 and 1520 cm^{-1}, respectively. The emergence of these features may be due to the low levels of H within the material compared to that found in the more rigorously studied a-C:H.

Fig. 5 shows the Raman spectrum from the sample deposited at $\approx$155 eV. Similar spectra were found for films deposited at ion energies of between 150 and 200 eV. The Raman spectrum is dominated by the G band at $\approx$1550 cm^{-1}, which also shows a weak shoulder characteristic of the D band at 1345 cm^{-1} (the peak at 970 cm^{-1} is due to the Si substrate). This result differs from that observed in ta-C where only the G band is observed [18]. The presence of a small D band in ta-C:H suggests the presence of some aromatic species within the film structure, in agreement with the 1520 cm^{-1} IR absorption in Fig. 4. However, the small I_D/I_G ratio ($\approx$0.3) suggests that there is negligible sp^2 clustering (5 Å) [19].
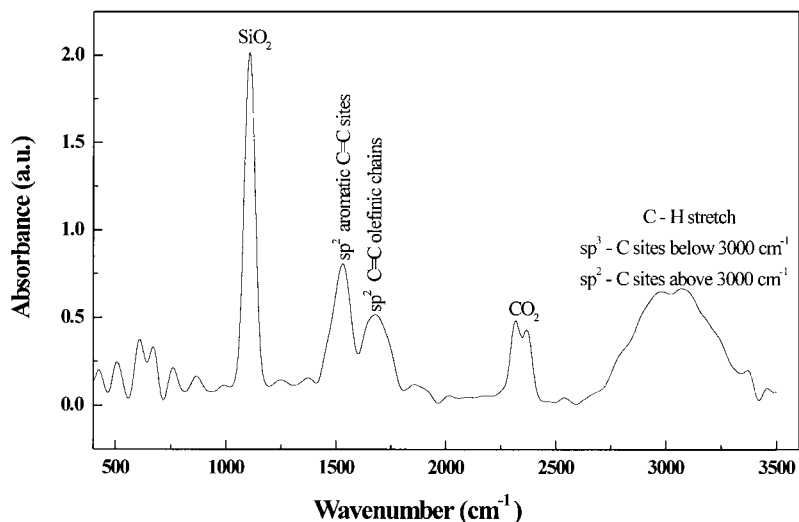
Fig. 4. FTIR spectrum obtained from the sample deposited at an ion energy of ≈155 eV

The lower density of these ta-C:H films compared with ta-C films deposited in a filtered cathodic vacuum arc [16] may be attributed to the termination of the sp^3 carbon sites within the network with hydrogen atoms. Thus, for high sp^3 carbon fractions and moderate hydrogen contents mass densities approaching 2.38 g/cm^3 were obtained.

Fig. 3 also showed the variation of the optical (Tauc) gap with the ion energy. When the ion energy exceeds the optimum energy, the sp^2 content within the film increases and the Tauc gap is reduced. This reduction in the optical gap is known to be dependent on the density and configuration of the sp^2 sites within the network, as the gap is
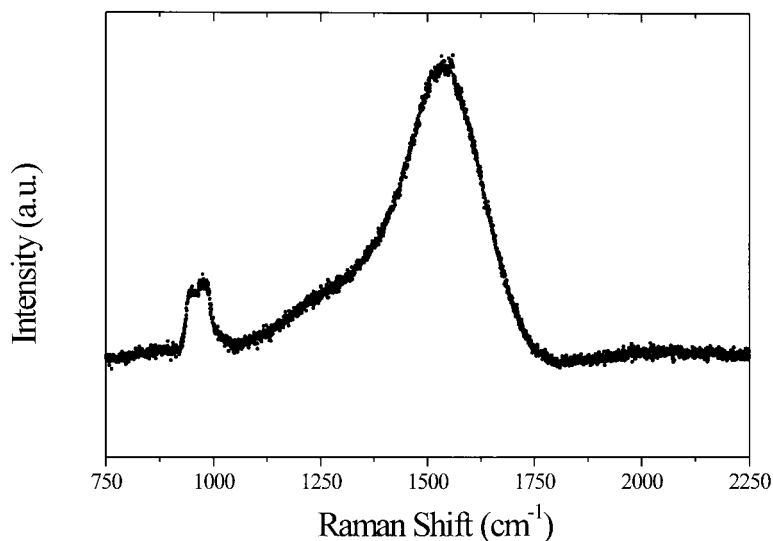

Fig. 5. Raman spectrum for the sample deposited at an ion energy of ≈155 eV

itself determined by the gap between the π states and the π^* states on the sp^2 sites [20, 21]. Furthermore, a simplified model presented previously [20] suggested that because of ion bombardment during deposition, the sp^2 cluster size is limited to between 2 and 10 sp^2 sites, thus permitting the formation of olefinic chains and small aromatic clusters within an sp^3 hybridized network. Such behavior would certainly be consistent with the FTIR and Raman results presented above, although at present there are no direct means of determining exact sp^2 cluster sizes in ta-C : H.

The AFM measurements (see Fig. 6) indicated that the as-deposited films were exceptionally smooth, with typical surface RMS roughness of less than 0.3 nm. Furthermore, no distinct differences in surface topography were observed for films deposited at ion energies of between 150 and 200 eV.

In a similar fashion, the coefficient of friction did not exhibit a dependence upon the ion energy within the film forming flux. However, as the humidity was raised from ambient levels (ca. <10% RH) up to approximately 50% RH, the coefficient of friction increased from 0.16 to 0.25 which compares with 0.05 to 0.5 for a-C : H [2, 22, 23]. The low friction of a-C : H in a dry environment has been attributed to the formation of a transfer layer of either graphite or a-C : H on the counter surface [2, 22, 23]. This transfer layer may become oxidised under high humidity conditions, leading to an increase in the observed coefficient of friction [22]. Unfortunately, the exact mechanism by which this process is thought to occur is as yet unknown. Similar frictional behavior is expected during the tribological testing of ta-C : H films. However, as ta-C : H is known to have a superior mechanical hardness when compared to a-C : H [4] it is conceivable that the formation of such a transfer layer is more difficult. Consequently, as the humidity levels rise, the variation in friction coefficient when compared with a-C : H is less likely to be significant.
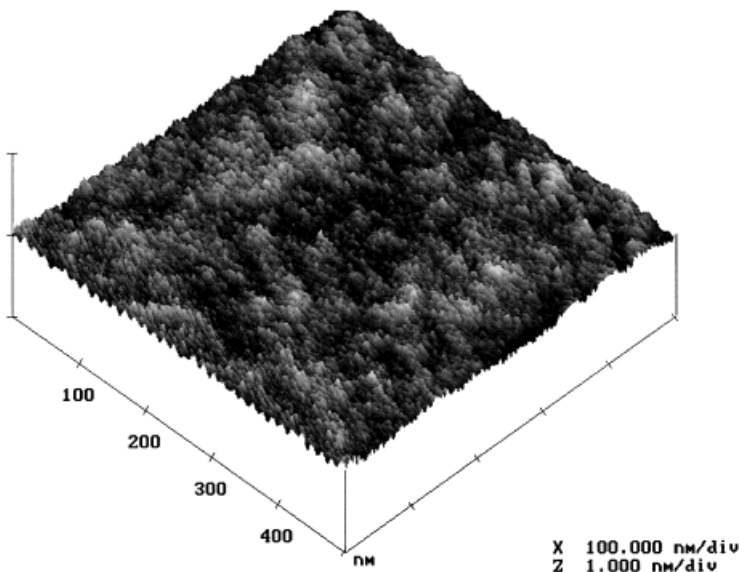

Fig. 6. Atomic force micrograph of a film deposited at $\approx$155 eV

The deposition of ta-C:H, as with ta-C, has been found to be controlled principally by the energy of the incident ion flux. Therefore, to a first order, the effect of neutral and radical species can be neglected and the deposition process may be described by a subplantation model of subsurface growth [24, 25]. It is commonly accepted that the predominant species in a low-pressure acetylene plasma is the $C_2H_2^+$ ion [4]. Upon impact at the growth surface the $C_2H_2^+$ ions fragment resulting in the formation of two daughter C^+ ions, the kinetic energies of which, according to the principle of conservation of momentum, are given by

$$E_C = \frac{m_C E_{ion}}{2m_C + m_H} = 0.46 E_{ion} \, , \tag{9}$$

where E_C and E_{ion} are the kinetic energies of the carbon daughter and the $C_2H_2^+$ ion species, respectively and m_C and m_H represent the atomic masses for carbon and hydrogen, respectively. Providing that the daughter C^+ ions are of sufficient energy, they may penetrate beyond the surface atomic layer as the collision cross-section decreases rapidly with an increase in ion energy. Following penetration these ions enter a subsurface interstitial position and increase the local density, thus promoting the formation of an sp^3 bonded network. Ions with energies below the threshold level, however, cannot penetrate and stick to the outer surface resulting in either sp^2 rich or polymeric a-C:H, whereas species of very high energy penetrate deep into the film and dissipate their excess energy as a thermal spike, which promotes the thermal relaxation of the sp^3 network back into the thermodynamically more stable sp^2 bonded state. Consequently, the resultant net increase in density through subplantation may be described by

$$\frac{\Delta\varrho}{\varrho_0} = \frac{f}{\left(\frac{1}{\Phi}\right) - f + 0.016p\left(\frac{E}{E_0}\right)^{5/3}} \, , \tag{10}$$

where E is the incident ion energy, ϱ_0 is the uncompressed density, Φ is the ion flux ratio, p is a material dependent parameter and E_0 is the activation energy of relaxation. f represents the penetration fraction, which can be calculated by the TRIM code [26] or approximated empirically as

$$f = 1 - \exp\left[-\frac{(E - E_1)}{E_2}\right] , \tag{11}$$

where E_1 is the penetration threshold and E_2 is a spread parameter. Typically for ta-C:H reasonable agreement between experimental and theoretical results may be obtained providing that $p = 0.1$, $\varrho = 1.9$ g/cm^3, $E_0 = 1.46$ eV, $E_1 = 57$ eV and $E_2 = 16$ eV per carbon atom. This can be shown if we consider the case of the acetylene plasma used to deposit the sample at a $C_2H_2^+$ ion energy of ≈ 162 eV. At an rf power and chamber pressure of 200 W and 2.5×10^{-3} mbar, respectively, the ion flux ratio of the deposition species is of the order of 0.25. The predicted density using equations (10) and (11) shown above is therefore ≈ 2.31 g/cm^3 whereas the actual density determined via electron energy loss spectroscopy is 2.38 g/cm^3. The similarity between the two results confirms that ta-C:H film deposition whilst using an ECWR plasma beam source occurs through the subsurface implantation of carbon ions into the growing film. However, this also implies that if the ion flux ratio is increased for example by operating at

lower pressures and higher rf powers, then films of higher density can be obtained. Furthermore, a deposition mechanism of this nature, rather than clustering and island growth from either chemisorbed or physisorbed species, is thought to result in the virtually atomically smooth films observed by AFM.

5. Conclusions

It has been demonstrated that continuous ta-C:H coatings have been deposited on silicon and quartz substrates, at deposition rates of up to 900 Å/min, using an electron cyclotron wave resonance plasma beam source. Under optimum conditions the sp^3 fraction, mass density, film stress, Tauc gap and refractive index were found to be 0.77, 2.38 g/cm^3, 8 GPa, 2.1 eV and 2.45, respectively. The results obtained from both FTIR and Raman analysis of the deposited material also suggested that the ta-C:H films were composed of sp^3 hybridized carbon bonded to both olefinic chains and aromatic rings. Hydrogen contents less than 33 at% were also observed. The dependence of the deposition rate on the ion current density also suggests an ion dominated growth process. This was also confirmed by the ion energy dependence of the deposited film properties. The low surface roughnesses, as determined by AFM, and the presence of a low coefficient of friction between 0.16 and 0.25 in both dry and humid conditions therefore indicates the suitability of the material in applications requiring enhanced tribological performance.

References

[1] J. ROBERTSON, Progr. Solid State Chem. **21**, 199 (1991).
[2] K. ENKE, H. DIMIGEN, and H. HUBSCH, Appl. Phys. Lett. **36**, 291 (1980).
[3] P. KOIDL et al., Mater. Sci. Forum **52**, 41 (1989).
[4] M. WEILER, S. SATTEL, T. GEISSEN, K. JUNG, H. EHRHARDT, V.S. VEERASAMY, and J. ROBERTSON, Phys. Rev. B **53**, 1594 (1996).
[5] S. SATTEL, J. ROBERTSON, and H. EHRHARDT, J. Appl. Phys. **82**, 1 (1997).
[6] D.R. MCKENZIE, D. MULLER, and B.A. PAILTHORPE, Phys. Rev. Lett. **67**, 773 (1991).
[7] H. EHRHARDT, R. KLEBER, A. KRUGER, W. DWORSCHAK, K. JUNG, I. MUHLING, F. ENGELKE, and H. METZ, Diamond Relat. Mater. **1**, 316 (1992).
[8] M. WEILER, S. SATTEL, K. JUNG, H. EHRHARDT, V.S. VEERASAMY, and J. ROBERTSON, Appl. Phys. Lett. **64**, 2797 (1994).
[9] M. WEILER, K. LANG, E. LI, and J. ROBERTSON, Appl. Phys. Lett, **72**, 1314 (1998).
[10] B. PFEIFFER, J. Appl. Phys. **37**, 1624, 1628 (1966).
[11] H. OECHSNER, Plasma Processing of Semiconductors, Ed. P.F. WILLIAMS, Kluwer Academic Press, Dordrecht 1990 (p. 157).
[12] R. KRIMKE and H.M. URBASSEK, J. Appl. Phys, **81**, 7163 (1997).
[13] F.F. CHEN, in: Introduction to Plasma Physics, 3rd ed., Plenum Press, New York 1977.
[14] P.J. FALLON, V.S. VEERASAMY, C.A. DAVIS, J. ROBERTSON, G.A.J. AMERATUNGA, W.I. MILNE, and J. KOSKINEN, Phys. Rev. B **48**, 4777 (1993).
[15] B.E. CHERRINGTON, Plasma Chem. and Plasma Processing **2**, 113 (1982).
[16] M. CHHOWALLA, J. ROBERTSON, C.W. CHEN, S.R.P. SILVA, C.A. DAVIS, G.A.J. AMARATUNGA, and W.I. MILNE, J. Appl. Phys. **81**, 139 (1997).

[17] B. Dischler, in: Europ. Mater. Res. Soc. Symp. Proc., Vol. 17, Les Editions de Physique, Les Ulis (France) 1987 (p. 189).
[18] S. Prawer, K.W. Nugent, Y. Lifshitz, G.D. Lempert, E. Grossman, J. Kulik, I. Avigal, and R. Kalish, Diamond Relat. Mater. **5**, 433 (1996).
[19] J. Schwan, S. Ulrich, V. Batori, H. Ehrhardt, and S.R.P. Silva, J. Appl. Phys. **80**, 440 (1996).
[20] J. Robertson, Diamond Relat. Mater. **4**, 297 (1995).
[21] T. Frauenheim, G. Jungnickel, V. Stephan, P. Blaudeck, S. Deutscmann, M. Weiler, S. Sattel, K. Jung, and H. Ehrhardt, Phys. Rev. B **50**, 7940 (1994).
[22] J. Meneve, E. Dekempeneer, S. Kuypers, R. Jacobs, and J. Smeets, Diamond Relat. Mater. **4**, 366 (1995).
[23] K. Enke, Thin Solid Films **80**, 227 (1981).
[24] Y. Lifshitz, S.R. Kasi, J.W. Rabalais, and W. Eckstein, Phys. Rev. B **4**1, 10468 (1990).
[25] J. Robertson, Diamond Relat. Mater. **2**, 984 (1993); **3**, 361 (1994).
[26] W. Eckstein, Computer Simulations of Ion Solid Interactions, Springer-Verlag, New York 1990.